The influence of apparatus stiffness on the results of cyclic direct simple shear tests on dense sand

Konstadinou, M.; Bezuijen, A.; Greeuw, G.; Zwanenburg, C.; van Essen, H. M.; Voogt, L.

DOI
10.1520/GTJ20190471

Publication date
2020

Document Version
Accepted author manuscript

Published in
Geotechnical Testing Journal

Citation (APA)
Konstadinou, M., Bezuijen, A., Greeuw, G., Zwanenburg, C., van Essen, H. M., & Voogt, L. (2020). The influence of apparatus stiffness on the results of cyclic direct simple shear tests on dense sand. *Geotechnical Testing Journal*, *44*(5), 1501-1525. https://doi.org/10.1520/GTJ20190471

ASTM INTERNATIONAL

Geotechnical Testing Journal

M. Konstadinou,[1] A. Bezuijen,[2,3] G. Greeuw,[3] C. Zwanenburg,[3,4] H. M. Van Essen,[3] and L. Voogt[3]

DOI: 10.1520/GTJ20190471

The Influence of Apparatus Stiffness on the Results of Cyclic Direct Simple Shear Tests on Dense Sand

Geotechnical Testing Journal

doi:10.1520/GTJ20190471 available online at www.astm.org

M. Konstadinou,[1] A. Bezuijen,[2,3] G. Greeuw,[3] C. Zwanenburg,[3,4] H. M. Van Essen,[3] and L. Voogt[3]

The Influence of Apparatus Stiffness on the Results of Cyclic Direct Simple Shear Tests on Dense Sand

Reference

M. Konstadinou, A. Bezuijen, G. Greeuw, C. Zwanenburg, H. M. Van Essen, and L. Voogt, "The Influence of Apparatus Stiffness on the Results of Cyclic Direct Simple Shear Tests on Dense Sand," *Geotechnical Testing Journal* https://doi.org/10.1520/GTJ20190471

ABSTRACT

A series of undrained cyclic direct simple shear (CDSS) tests on dense Toyoura sand has been performed with the aim to investigate the influence of the stiffness of the DSS device on test results. To this end, springs were installed to reduce deliberately the stiffness of the apparatus. It is shown that the cyclic resistance of the sand depends strongly on the rigidity of the apparatus frame. In particular, as the stiffness of the DSS device increases, the number of loading cycles required to reach liquefaction decreases. This pronounced apparatus–stiffness dependence is of great practical concern in geotechnical engineering because it directly implies that the CDSS response of a soil sample can be predominantly controlled by the stiffness of the apparatus and not by the soil behavior alone. In addition, the test results indicate that the effect of equipment compliance in cyclic undrained DSS testing can be minimized when the ratio of the stiffness of the tested sand sample to the stiffness of the apparatus has a significantly low value.

Keywords

direct simple shear tests, apparatus stiffness, cyclic testing, dense sands

Manuscript received December 22, 2019; accepted for publication July 1, 2020; published online xxxx xx, xxxx.

[1] Geo-Engineering Section, Deltares, Boussinesqweg 1, Delft 2629 HV, The Netherlands (Corresponding author), e-mail: maria.konstantinou@deltares.nl, https://orcid.org/0000-0001-9488-0798

[2] Department of Civil Engineering, Ghent University, Technologiepark 68, Zwijnaarde B-9052, Belgium

[3] Geo-Engineering Section, Deltares, Boussinesqweg 1, Delft 2629 HV, The Netherlands

[4] Geo-Engineering Section, Delft University of Technology, Mekelweg 5, 2628 CD, Delft, The Netherlands

Nomenclature

CSR = cyclic stress ratio $\left[\left(\frac{\tau_{SA}}{\sigma_{vc}}\right)\right]$

D_r = relative density

e_{min}, e_{max} = minimum and maximum void ratios

G_s = specific gravity

$K_{eff}^{(K_1+K_2)}$ = stiffness of the part of the direct simple shear apparatus outside the linear variable differential transducer measurement area
K_i = direct simple shear apparatus stiffness
K_0 = coefficient of earth pressure at rest
K_1 = stiffness of the spring cell
K_2 = stiffness of the load cell
K_3 = stiffness of the load piston
K_s = stiffness of the soil sample
N = number of cycles
N_f = number of cycles to develop $\gamma_{SA} = 5$ %
γ = shear strain
γ_{SA} = single amplitude cyclic shear strain
Δx_e = external axial displacement measured with the linear variable differential transducer
Δx_i = internal axial displacement measured with the motor encoder
$\Delta x_{K_3}^{el}$ = elastic displacement of the load piston
Δx_s^{el} = elastic displacement of the soil sample
Δx_s^{pl} = plastic displacement of the soil sample
$\Delta \delta_s^{el}$ = elastic deformation of the soil sample
$\Delta \delta_s^{pl}$ = plastic deformation of the soil sample
$\Delta \varepsilon_{axial,e}$ = external axial strain measured with the linear variable differential transducer
$\Delta \varepsilon_{axial,i}$ = internal axial strain measured with the motor encoder
$\Delta \varepsilon_v$ = volume change of the soil sample
$\Delta \sigma_v'$ = vertical stress reduction
$\Delta \sigma_{v(N=1)}^{'(Motor)}$ = vertical stress reduction at $N = 1$ of a motor-controlled cyclic direct simple shear test
$\Delta \sigma_{v(N=1)}^{'(LVDT)}$ = vertical stress reduction at $N = 1$ of a linear variable differential transducer–controlled cyclic direct simple shear test
$\Delta \sigma_{v,t}'$ = theoretical vertical stress reduction
$\Delta \sigma_{v,m}'$ = measured vertical stress reduction
σ_v' = vertical effective stress
σ_{vc}' = vertical effective stress at the end of consolidation
σ_{vi}' = vertical effective stress at preparation stage
σ_{vu}' = vertical effective stress at the end of the unloading stage
τ_{SA} = single-amplitude cyclic shear stress
τ, τ_{xy} = shear stress
ϕ' = mobilized friction angle
ϕ_{FL}' = mobilized friction angle at failure line

Introduction

The direct simple shear (DSS) apparatus has been originally developed in 1936 by the Royal Swedish Geotechnical Institute (Kjellmann 1951), whereas other types of DSS devices have been evolved from the original such as the Cambridge University and the Norwegian Geotechnical Institute (NGI) DSS devices (Roscoe 1953; Bjerrum and Landva 1966).

DSS testing simulates more realistically plane strain conditions that involve the rotation of principal stresses while it allows for the application of initial static shear to represent sloping ground conditions. In addition, DSS testing is known for its ability to replicate the field conditions during earthquake/cyclic loading more realistically, as cyclic shear stress is applied to the horizontal plane of the soil sample. The cyclic direct simple shear (CDSS) test is thus often used to determine the cyclic properties and the liquefaction potential of sand deposits (Peacock and Seed 1968; Finn, Pickering, and Bransby 1971; Ishihara and Yamazaki 1980; Vaid and Chern 1985; Vaid and Sivathayalan 1996; Wijewickreme, Sriskandakumar, and Byrne 2005; Andersen 2009; Cappellaro et al. 2017).

In the recent past, a cooperative testing program that concerned the performance of CDSS tests on sand samples for evaluating the bearing capacity of an offshore installation was conducted. The CDSS tests were performed at two different laboratories that were equipped with DSS devices constructed by different manufacturers. Even though the tests were performed on the same sand under identical conditions, quite different results were obtained. These results indicated that the stiffness of the components of the DSS apparatus might play a role, as the DSS devices used for testing had different frame stiffnesses. It should be mentioned that for confidentiality reasons, no reference is given herein for the conducted testing program.

In this study, a test series was performed in which the stiffness of the DSS apparatus was changed deliberately and its influence on the cyclic behavior of dense Toyoura sand samples was evaluated. The cyclic behavior is explored in terms of effective vertical stress, axial strain, and volume change development during DSS loading. It should be emphasized that only dense sand samples are considered in this study as it is expected that the influence of apparatus stiffness will be more pronounced when testing involves stiff materials.

THEORY

The CDSS test is used to investigate the possible liquefaction of sand deposits under cyclic loads. The basic principle is that under undrained conditions cyclic loading will lead to very low or even vanishing effective stresses and large deformations of the sand sample. In the field, (nearly) undrained conditions can be achieved depending on the rate of loading in relation to the rate of pore pressure dissipation. When no groundwater flow is possible, there cannot be any volume change because both pore water and sand grains are nearly incompressible. The DSS apparatus uses the conservation of volume by inhibiting any volume strain changes of the sample during shear. Ring stacks or a wire-reinforced membrane prevents lateral strain. A vertical load piston fixes the height of the sample (see **fig. 1**). During a DSS test, the load piston is lowered until the required vertical stress on the sample is reached. The effective horizontal stress is not prescribed, and it is assumed to be equal to K_0 times the effective vertical stress. A horizontal cyclic loading is applied, inducing a shear strain in the sample. During horizontal loading, the load piston in the vertical direction is fixed and thus constant volume conditions are achieved. For contractive sands, cyclic loading will lead to a reduction of the sample's height and because the volume is fixed, there will be some elastic unloading of the sample, resulting in a decrease in the vertical stress, which is measured as a force reduction on the load piston. Continuous cyclic loading will result in vanishing of the effective stress and to liquefaction of the sand sample. Following Dyvik et al. (1987), the imposed constant height condition is considered to mimic undrained behavior and the change in vertical stress during shearing is assumed to be equal to the excess pore water pressure. Because of the nature of the DSS test, liquefaction can be reached even with dry sand because, as is explained, the constant volume is not achieved by the pore water pressure but by the imposed constant volume of the sample holder.

In reality, however, the apparatus will have a finite stiffness. This means that a stress reduction, as will occur during cyclic loading, will lead to some volume change of the sample. Because of the stress reduction, there will be an elastic deformation of the load piston, resulting in its movement and to a change of the sample's volume. This change will depend on the stiffness of the apparatus in relation to the stiffness of the soil sample. It is hypothesized that differences in the apparatus stiffness can be one of the predominant factors to explain the different CDSS test results found by different laboratories. To test this hypothesis, experiments were performed in which the stiffness of the apparatus was varied and its influence on the number of loading cycles to failure was investigated. Here, it is assumed that the vertical deformation is dominant, and it is influenced by the varying stiffness of the apparatus.

FIG. 1 Pictures of Deltares direct simple shear device: 1, water tank; 2, precision weighing balance; 3, motor encoder; 4, horizontal cross member; 5, vertical column; 6, vertical LVDT; 7, horizontal LVDT; 8, spring cell unit; 9, vertical force load cell; 10, load piston; 11, soil sample enclosed with membrane and ring stacks; 12, horizontal force load cell; 13, shear slide plates.

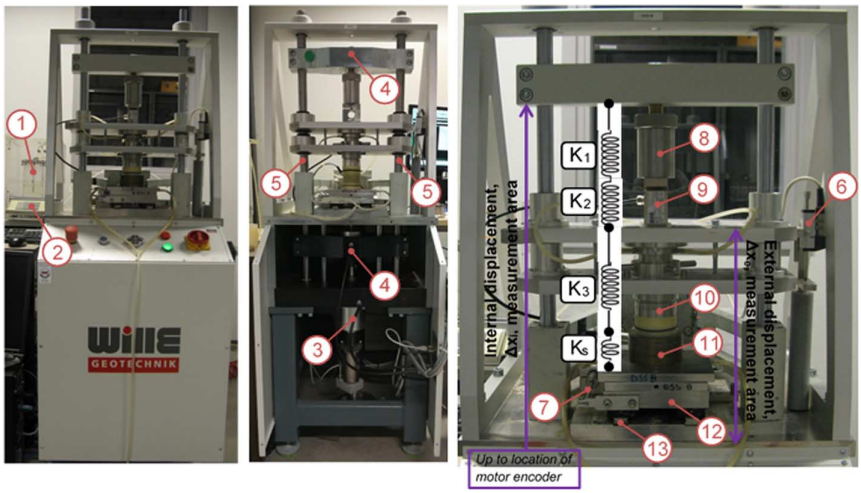

However, the method of lateral confinement of the samples may also influence their stiffness in the horizontal direction, as will be discussed later.

Testing Setup

The tests were carried out in the geotechnical laboratory of Deltares in The Netherlands using CDSS apparatuses manufactured by Wille. Tests were performed on cylindrical samples having a diameter of 63 mm and a height at preparation of approximately 20 mm. These dimensions give a high diameter to height ratio to minimize the nonuniformity of stress and strain in the sample (Boulanger and Seed 1995; Matsuda et al. 2004; Kim 2009; Li et al. 2017). A picture of the Deltares CDSS apparatus employed in this study is shown in **figure 1**.

The horizontal displacement is monitored using a linear variable differential transducer (LVDT), whereas the horizontal load is measured using a load cell with a maximum reach of 5 kN, located directly below the sample. The vertical axis includes one 5-kN load cell for controlling and measuring the vertical load. During testing, two independent vertical displacement measurements are recorded. That is the vertical displacement as measured with the LVDT and with the motor encoder (see **fig. 1**). To differentiate among the two measurements, the terms external displacement, Δx_e, when referring to the LVDT measurements and internal displacement, Δx_i, when referring to the motor encoder measurements, are adopted in this study.

The horizontal and vertical LVDTs have a range of −2.5 to +2.5 mm and an accuracy of ±0.15 % of full range. The axial and horizontal load cells are accurate to ± 1.6 N and ±3.3 N, respectively. For the sample dimensions used in this study, this corresponds to an accuracy of ±0.51 kN/m^2 and ±1.06 kN/m^2.

For measuring volume changes of the samples during testing, the DSS apparatus is equipped with a water tank connected with a closed system to the inlet at the top of the sample. The water tank is placed on a precision weighing balance that continuously monitors the inflow/outflow of fluid in the water tank. The balance, manufactured by Mettler Toledo, has a maximum capacity of 4,100 g and a readability down to 0.01 g.

According to ASTM D6528-17, *Standard Test Method for Consolidated Undrained Direct Simple Shear Testing of Fine Grain Soils*, in undrained, constant volume, DSS tests, the height of the sample must be maintained practically constant during shear (maximum tolerated change in sample height of 0.05 %). This was attempted to

be achieved either by (i) mechanically locking the height at the vertical motor encounter level (passive height control) and (ii) adjusting the vertical movement in a displacement-controlled mode to eliminate any displacement measured by the LVDT transducer (active height control). For the passive height control tests, the horizontal cross members and the vertical columns in **figure 1** are locked at the motor encounter level. For the active height control tests, the signal from the LVDT transducer is fed back to a PC software, which controls the vertical movement to prevent LVDT displacement measurements. Tests performed according to height control method (i) and (ii) will be referred to in this study as "motor controlled" and "LVDT controlled" tests, respectively.

For the purposes of this study, it is considered that the applied DSS apparatus, as any apparatus, has a finite stiffness. This finite stiffness is schemed as a combination of springs in series as illustrated in **figure 1**. The stiffness of the apparatus components is expressed via the stiffness factors K_1, K_2, K_3 and K_s, which correspond to the stiffness of the spring cell/reaction frame, load cell, load piston/shear load cell/shear slide plates and soil sample, respectively. This is a simplified approach, and it should be noted that, overall, K_1 and K_2 reflect the stiffness of the part of the apparatus outside the vertical LVDT measurement area, whereas K_3 reflects the stiffness of the part of the apparatus within this area. In this article, stiffness is presented in kPa/mm. This way of presenting allows for a direct comparison of various components in the pressure (kPa) and displacement (mm) units normally used in geotechnical testing.

For isolating the effect of apparatus stiffness, it is critical in this study to perform a series of tests under identical testing conditions by altering solely the stiffness of the apparatus. The latter can be achieved by changing the stiffness factor, K_1, via the use of spring rings fixed into the spring cell unit located at the top part of the apparatus. Because K_1 is outside the vertical LVDT measurement, it should have no influence on the LVDT-controlled tests in contrast to the motor-controlled tests. Four different apparatus stiffness settings are mobilized. Specifically, the apparatus has been tested without the addition of springs ("no springs") and under three spring ring settings ("setting A," "setting B," and "setting C"). The exact combination of the spring rings corresponding to each setting is shown in **figure 2**.

Materials and Testing Procedure

A standard research sand, the Toyoura sand, is used in this study. It is a clean fine uniform sand and has been extensively used in previous studies (e.g., Tatsuoka, Muramatsu, and Sakaki 1982; Toki et al. 1986; Kiyota et al.

FIG. 2 Spring ring setting combinations mobilized in this study.

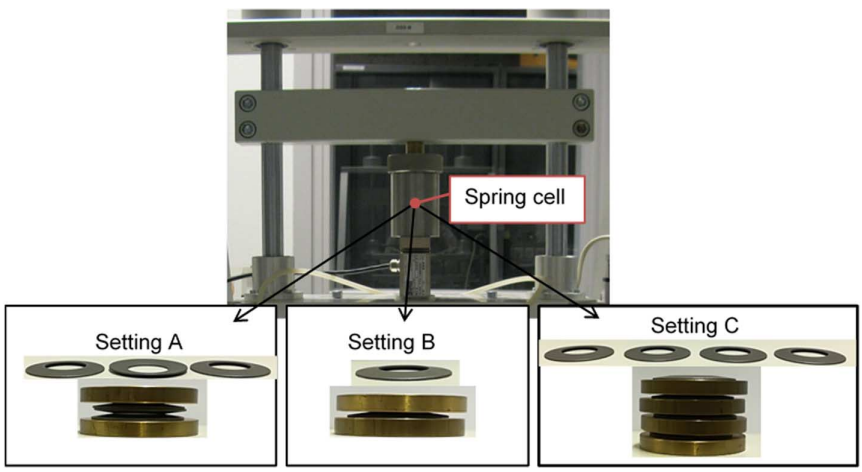

2008; Chiaro, Koseki, and Sato 2012). It has subangular- to angular-shaped particles, minimum (e_{min}) and maximum (e_{max}) void ratios of 0.561 and 0.975, respectively, and specific gravity $G_s = 2.635$ (Kiyota et al. 2008).

All samples were prepared by the air pluviation method (Mulilis et al. 1977). Air-dry sand is poured from a nozzle with a constant drop height into a mold. Densification of the samples was achieved by compaction in one layer using a dead weight of 750 g falling on the top of the sample from a height of 30 cm until a constant sample height of 20 mm is reached. For all tested samples, this was achieved after 8 weight falls. To avoid distortion, the samples were laterally supported during compaction by an aluminum ring. The relative density of the samples after preparation was $D_r = 80 \pm 3$ %.

The samples were saturated under a seating pressure of 10 kPa by flushing carbon dioxide through the voids among the sand particles and by subsequently percolating deaired water from the bottom to the top of the sample. The amount of deaired water percolated is of the order of twice the sample's total volume. The samples were saturated to allow measurement of volume change during consolidation and shearing. The volume change is determined from the amount of water that is expelled from or drawn into the sample; the latter is recorded by the weighing balance employed in this study.

After saturation, the samples were consolidated to $\sigma'_{vc} = 200$ kPa starting from an initial stress state at preparation of $\sigma'_{vi} = 10$ kPa. After a consolidation period of 1 h, the samples were subjected to two unloading-reloading vertical stress loops. The samples were unloaded to $\sigma'_{vu} = 100$ kPa and reloaded back to the consolidation stress level of $\sigma'_{vc} = 200$ kPa with a rate of 20 kPa/min. These loops were conducted to allow estimation of the sample's stiffness. Following Andersen (2009), the samples were thereafter presheared under drained conditions at $\frac{\tau_{SA}}{\sigma'_{vc}} = 0.03$ for 400 cycles, where τ_{SA} is the single-amplitude cyclic shear stress, with a frequency of 1 Hz. Samples were presheared (i) to replicate the in situ stress history of soils subjected to drained preshearing prior to the main design event (i.e., wave-induced loading of seabed sand deposits) and (ii) to mitigate sample inhomogeneity by leveling out stress concentrations arising from sample preparation and consolidation (Quinteros et al. 2017).

After preshearing, the samples were subjected to stress-controlled cyclic loading under undrained simple shear conditions. Cyclic loading was applied by way of a sinusoidal shear load at a frequency of 0.1 Hz.

Typical graphs showing the variation of vertical stress, σ'_v and shear stress τ during consolidation and preshearing of the samples are illustrated in **figure 3**.

The samples in this study were laterally confined by means of a rigid metal ring stacks enclosing an unreinforced rubber membrane. The membrane used has a thickness of 0.25 mm. A limited number of tests was performed on samples confined with a wire-reinforced, type C 1.50 membrane manufactured by Geonor. This type of wire-reinforced membrane has, for the sample's area in this study, a published vertical stress capacity higher than 1,000 kPa (McGuire 2011).

Tests were also performed on two apparatuses, referred to as DSS A and DSS B, to examine the influence of testing device on the experimental test results. It should be noted that apparatus DSS B is less stiff than DSS A. Most of the test results presented in this article are from DSS A.

Table 1 summarizes the testing conditions of all the tests reported in this study.

COMPLIANCE TESTS AND SAMPLE STIFFNESS

Compliance Tests on a Dummy Aluminum Sample

Compliance tests were conducted on a 20-mm-thick dummy aluminum sample, which was subjected to three loading-unloading vertical load loops within the stress range of 10–1,400 kPa. In **figure 4A** and **4B**, the applied vertical stress loops are plotted with respect to the internal, Δx_i, and external, Δx_e, vertical displacement measurements, respectively. Because of the nonlinear behavior of the compliance curves, **figure 4C** and **4D** are produced, which include only the part of the compliance curves related to the stress level of interest in this study close to the samples' consolidation level of 200 kPa. The dashed lines in **figure 4C** and **4D** are the best fit lines to the experimental data with their slope corresponding to the apparatus stiffness as this is assessed from the

FIG. 3

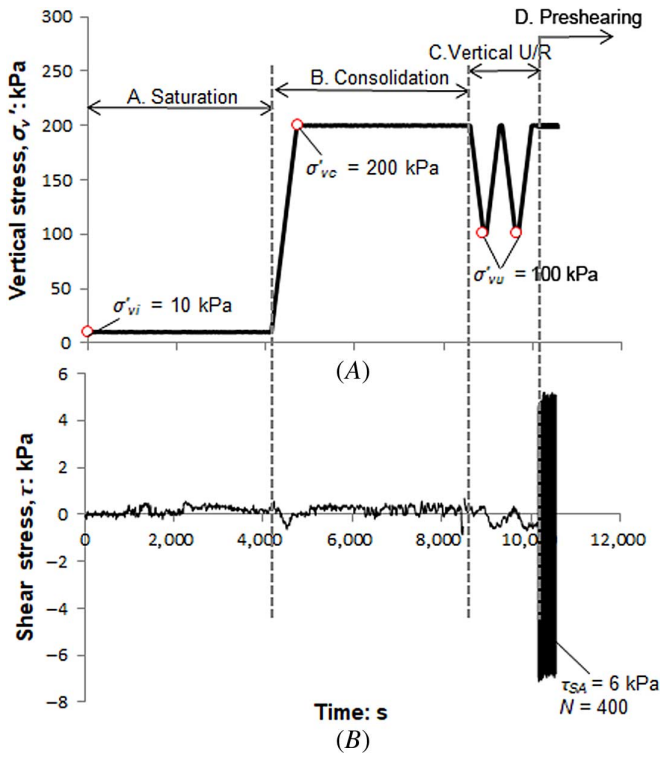

Variations in (*A*) vertical effective stress, σ_v'; (*B*) shear stress, τ, during saturation, consolidation, vertical unloading-reloading, and preshearing of dense Toyoura sand samples.

internal (fig. 4C) and external displacement recordings (fig. 4D). The former stiffness will be denoted in this study as K_i, and it is expressed as

$$\frac{1}{K_i}=\frac{1}{K_1}+\frac{1}{K_2}+\frac{1}{K_3} \tag{1}$$

The apparatus stiffness computed from the external displacement measurements corresponds directly to the stiffness of the lower part of the apparatus that belongs in the measurement area of the LVDT, K_3. The stiffness of the upper part of the apparatus can be deducted from equation (1) as follows:

$$\frac{1}{K_{eff}^{(K_1+K_2)}}=\frac{1}{K_i}-\frac{1}{K_3} \tag{2}$$

The derived K_i, K_3, and $K_{eff}^{(K1+K2)}$ values are summarized per spring setting combination in Table 2. The behavioral pattern in figure 4A and 4C clearly demonstrates that the use of springs alters to a significant degree the stress-strain response of the system, as far as Δx_i measurements are concerned, up to the vertical stress level of 400 kPa; the calculated stiffness, K_i, fluctuates from 119 kPa/mm (setting C) up to 2,970 kPa/mm (no springs). Intermediate stiffness values are measured for the spring setting A ($K_i = 162$ kPa/mm) and spring setting B ($K_i =$ 844 kPa/mm). Beyond the stress level of 400 kPa, the impact of springs diminishes, and the response of the system is comparable to the condition without springs. In contrast, the stress-strain response in figure 4B and 4D is not distinctly dependent on the type of spring used and an approximately unique apparatus stiffness is obtained irrespective of the spring setting ($K_3^{aver} = 6{,}300$kPa/mm). This is the expected trend, as the external displacement measurements reflect the compliance of the system only for the part of the apparatus components that are within the measurement area of the LVDT where the springs do not play any role. On the other hand, the internal

TABLE 1
Sample characteristics

Test	Spring Setting	Height Control	DSS Apparatus	Confinement Method	Loading Type	Volume Data	D_r, %	CSR	N_f
NS-1	NS	LVDT	A	RS	C	No	82	0.10	41
NS-2	NS	LVDT	A	RS	C	No	80	0.10	30
NS-3	NS	LVDT	A	RS	C	Yes	82	0.10	39
NS-4	NS	LVDT	A	RS	C	No	81	0.10	43
NS-5	NS	LVDT	B	RS	C	No	83	0.10	36
NS-6	NS	LVDT	B	RS	C	No	81	0.10	32
NS-7	NS	LVDT	A	RS	C	No	83	0.15	2
NS-8	NS	LVDT	A	RS	C	No	81	0.13	6
NS-9	NS	LVDT	B	RS	C	No	79	0.13	6
NS-10	NS	LVDT	B	RS	C	No	81	0.12	9
NS-11	NS	Motor	A	RS	C	No	82	0.10	106
NS-12	NS	LVDT	A	RS	M	No	80	…	…
NS-13	NS	LVDT	A	RM	C	Yes	79	0.10	105
NS-14	NS	LVDT	A	RM	C	Yes	82	0.10	86
NS-15	NS	LVDT	A	RM	C	Yes	78	0.17	8
NS-16	NS	LVDT	A	RM	C	No	82	0.15	18
A-1	A	LVDT	A	RS	C	No	78	0.10	26
A-2	A	LVDT	A	RS	C	No	82	0.10	39
A-3	A	Motor	A	RS	C	No	81	0.10	>2,000
B-1	B	LVDT	A	RS	C	No	81	0.10	33
B-2	B	Motor	A	RS	C	No	81	0.10	921
C-1	C	LVDT	A	RS	C	No	83	0.10	30
C-2	C	LVDT	A	RS	C	No	79	0.10	17

Note: A = spring setting A; B = spring setting B; C = spring setting C; N_f = number of cycles required to develop single amplitude of shear strain, $\gamma_{SA} = 5$ %; NS = no springs; RM = reinforced membrane; RS = ring stacks. Loading type: C = cyclic; M = monotonic.

displacement measurements capture the response of the whole apparatus frame, and this results, under a certain vertical stress, in higher values than the LVDT measured external displacements, even when no springs are used ($K_i^{No\text{-}springs} = 2{,}970$ versus $K_3^{No\text{-}springs} = 6{,}300$kPa/mm).

It should be pointed out that the 20-mm height aluminum sample used in the compliance tests has an extremely high modulus of elasticity of approximately 71 GPa, corresponding to a stiffness of 3.6 GPa/mm, and its influence on the stiffness values given in Table 2 is deemed to be insignificant.

Compliance Tests on Sand Samples

In order to evaluate the sand sample's stiffness, the vertical stress during the unloading-reloading testing phase of the samples (stage C in fig. 3) is plotted versus the external displacement in figure 5. Note that to keep figure 5 clear, only test data from eight samples are presented, whereas a direct comparison of the data is facilitated by shifting the external vertical displacement of the samples at the start of the first unloading-reloading phase to the same initial value of 0.25 mm. The dashed lines indicate that upper and lower stiffness boundary values can be obtained, which in principle reflect the effective stiffness, $K_{eff}^{K_3+K_s}$, given by

$$\frac{1}{K_{eff}^{K_3+K_s}} = \frac{1}{K_3} + \frac{1}{K_s} \tag{3}$$

The $K_{eff}^{K_3+K_s}$ stiffness varies within the range of 2,700–4,980 kPa/mm. The stiffness of $K_3$was determined to be 6,300 kPa/mm. The sample stiffness values, K_s, are determined by equation (3) because

FIG. 4 Compliance curves for different spring settings in apparatus DSS A. Effective vertical stress, σ_v', against (*A*), (*C*) internal vertical displacement, Δx_i; (*B*), (*D*) external vertical displacement, Δx_e.

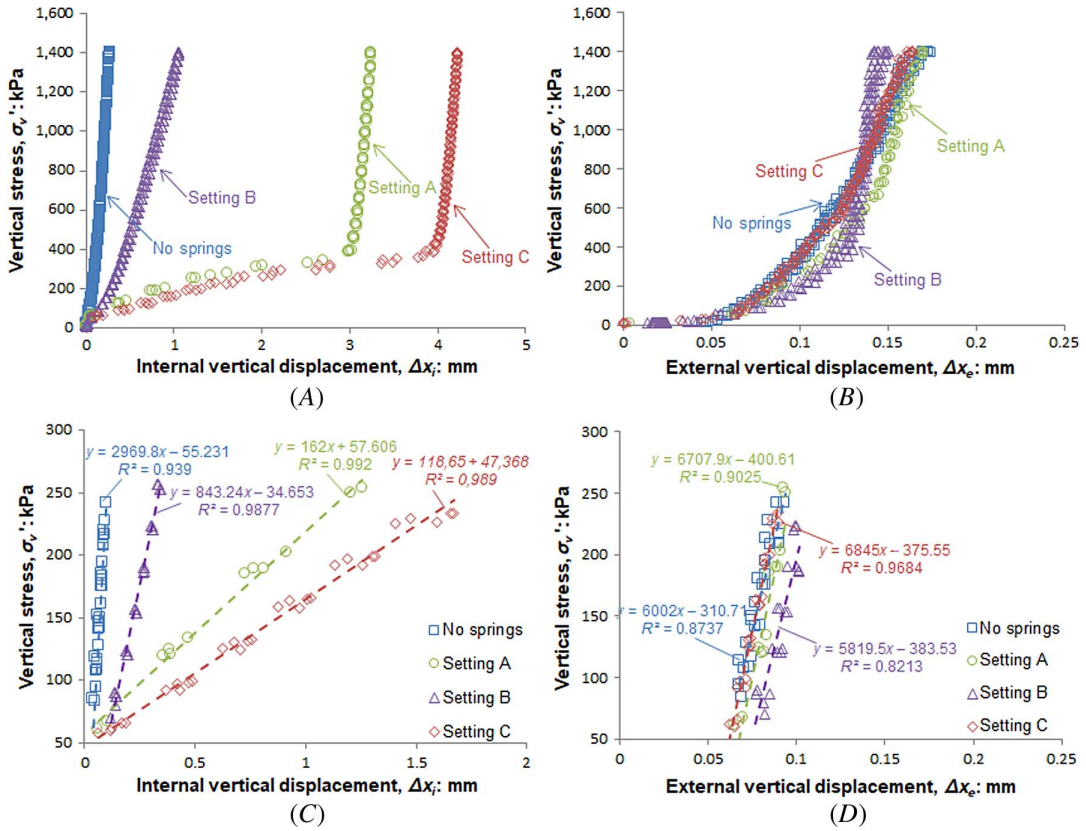

TABLE 2
Summary of stiffness properties for apparatus DSS A

Spring Combination	K_1, kPa/mm	K_3, kPa/mm	$K_{eff}^{(K_1+K_2)}$, kPa/mm	$K_{eff}^{(K_3+K_s)}$, kPa/mm	K_s, kPa/mm
No springs	2,970	5,800–6,800	5,619	2,700–	4,725–
Setting A	162	An average value of 6,300	166	4,980	23,768
Setting B	844	is considered in the analysis	975		
Setting C	119	of the data	121		

$$\frac{1}{K_s} = \frac{1}{K_{eff}^{(K_s+K_3)}} - \frac{1}{K_3} \tag{4}$$

and given together with the $K_{eff}^{K_3+K_s}$ values in Table 2.

The stiffness of the sand sample itself varies between 4,725 and a very high 23,770 kPa/mm. It should be noted that this determination is not very accurate because two values are subtracted, but the values found indicate that the stiffness of the sand sample is in the order of magnitude of the stiffness of the apparatus, even with external control.

The high stiffness of the sand sample suggests that very small deformations can have a significant influence on the vertical stress. As can be seen from figure 5, a vertical movement of 0.02 to 0.05 mm causes a drop in vertical effective stress of 100 kPa.

FIG. 5

Variation in effective vertical stress, σ_v', with external vertical displacement, Δx_e, during the unloading-reloading phase of the samples.

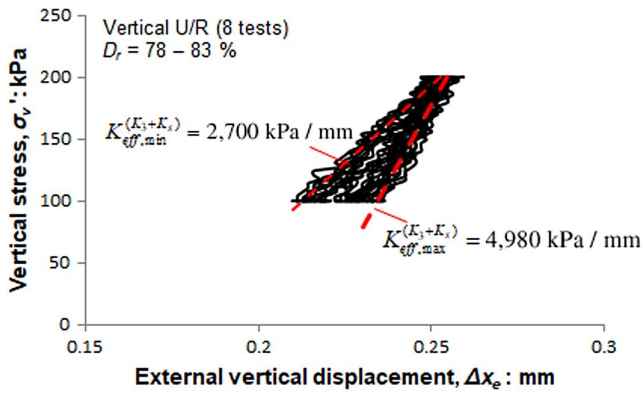

FIG. 6 Typical undrained cyclic simple shear response of dense ($D_r \sim 80$ %) Toyoura sand samples: (*A*) and (*B*) effective stress paths at $\tau_{xy} = \pm 20$ kPa and $\tau_{xy} = \pm 30$ kPa, respectively; (*C*) and (*D*) shear stress against shear strain at $\tau_{xy} = \pm 20$ kPa and $\tau_{xy} = \pm 30$ kPa, respectively.

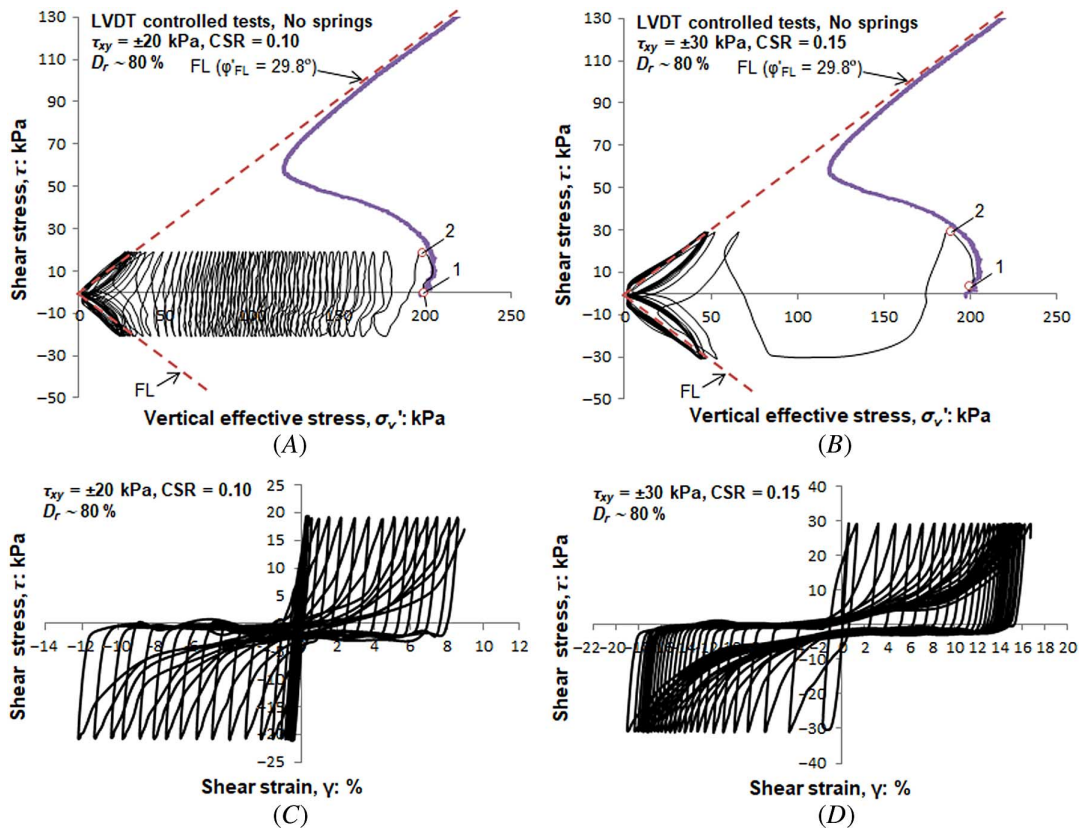

Description of CDSS Test Results

RESPONSE TO CYCLIC LOADING OF DENSE TOYOURA SAND SAMPLES TESTED UNDER LVDT AND MOTOR CONTROL HEIGHT CONDITIONS FOR DIFFERENT APPARATUS STIFFNESSES

Typical results for the tested dense Toyoura sand samples subjected to cyclic loading under LVDT-controlled conditions and in the absence of springs are illustrated in figure 6 for two different cyclic amplitude stress levels, $\tau_{xy} = \pm 20$ and ± 30 kPa. Plotted on figure 6A and 6B are the effective stress paths in the $\tau - \sigma_v'$ space, whereas figure 6C and 6D show the stress-strain response of the samples. In figure 6A and 6B, the stress path followed by a sample of similar density under monotonic simple shear loading has been included. The failure line (FL) defined from the monotonic test is also drawn together with its symmetrical line with respect to the mean effective vertical stress axis.

The cyclic effective stress paths appear to be bounded initially by the monotonic stress path (points 1–2), whereas at the final stage of loading, the samples show cyclic mobility characteristics (Castro 1975; Castro and Poulos 1977) as the cyclic stress path climbs up the FL at the expense of large shear strains. It is also interesting to note in figure 6A and 6B that the first loading cycle is wider than subsequent cycles, possibly because of significant particle rearrangement at the start of shearing. Similar features of behavior have been observed for dense sands subjected to cyclic torsional simple shear loading (Georgiannou and Tsomokos 2008; Konstadinou and Georgiannou 2013).

In figure 7, the number of cycles, N_f, required to develop a single-amplitude shear strain of $\gamma_{SA} = 5\%$ is plotted versus the internal apparatus stiffness, K_i, for the case of LVDT-controlled tests performed under different

FIG. 7

Relationship between number of cycles to develop a single amplitude of shear strain of $\gamma_{SA} = 5$ % and internal apparatus stiffness, K_i: (*A*) LVDT- and (*B*) motor-controlled tests on Toyoura sand samples at $D_r \sim 80$ % and $\tau_{xy} = \pm$ 20 kPa.

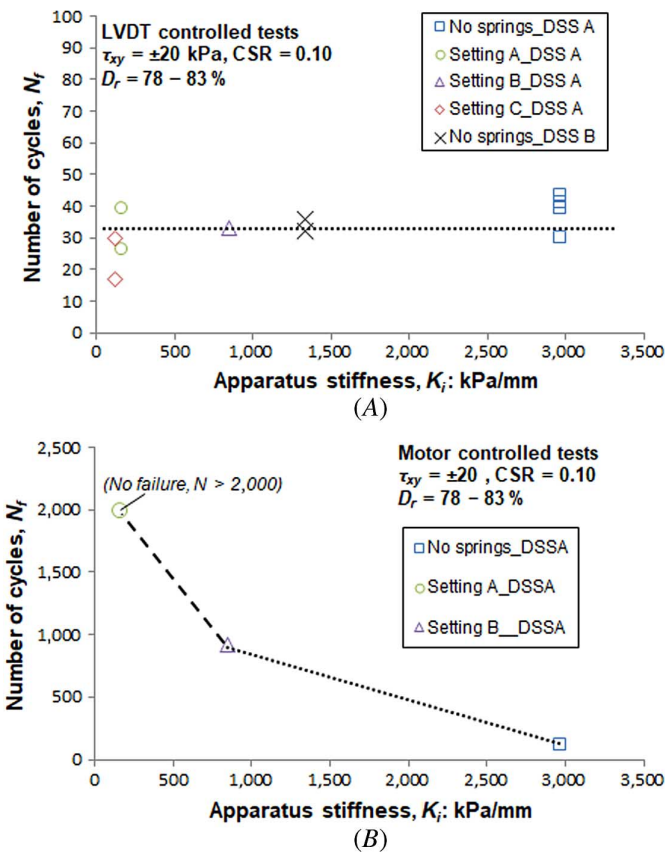

spring settings combinations on apparatus DSS A and DSS B. The resistance to cyclic loading is not influenced by the apparatus stiffness with an average $N_f = 33$ obtained regardless of the spring setting used (no springs, setting A, setting B, and setting C). Nevertheless, a scattering in the data exists, which can be attributed to some extent to small differences in the density state of the samples ($D_r = 78$–83 %). It should be highlighted that the relatively small height of the DSS samples poses difficulties in accurately estimating the density of the samples. Overall, the scattering of the test data in **figure 7A** can be a measure of the sensitivity of the CDSS response obtained from tests performed under identical conditions following a standardized testing procedure.

A completely different picture is illustrated in **figure 7B** for the motor-controlled tests where the number of cycles required to reach $\gamma_{SA} = 5\%$ decreases by more than 95 % when the apparatus stiffness increases from 162 (setting A) to 2,970 kPa/mm (no springs). A direct comparison between the LVDT- and motor-controlled $\gamma_{SA} - K_i$ curves is given in **figure 8A**. This figure clearly demonstrates that there is a significant difference in the resistance to cyclic loading between the two modes of testing. Motor-controlled tests exhibit a higher cyclic resistance, which is significantly enhanced as the apparatus stiffness decreases. These results demonstrate that LVDT (active) height-controlled tests should be preferred over motor (passive) height-controlled tests. For the former, the LVDT measurements should be limited to the sample alone or the LVDT transducer should be located as closely as possible to the sample.

The cyclic resistance curve as obtained from the LVDT controlled tests in this study at $\tau_{xy} = \pm 20$ kPa is shown in **figure 8B** together with the results of other studies, which include data on dense Toyoura sand samples ($D_r = 80$ %) reported by Tatsuoka, Muramatsu, and Sakaki (1982) and Toki et al. (1986). The former study refers to cyclic torsional simple shear tests, whereas the latter study refers to cyclic triaxial tests. The data in **figure 8B**

FIG. 8

Cyclic direct simple shear tests on dense ($D_r \sim 80$ %) Toyoura sand samples performed on apparatus DSS A and DSS B: (*A*) comparison between number of cycles and internal apparatus stiffness, K_i, curves of LVDT- and motor-controlled tests; (*B*) relationship between cyclic stress ratio, CSR, and number of cycles for cyclic triaxial, torsional simple shear, and LVDT-controlled direct simple shear tests.

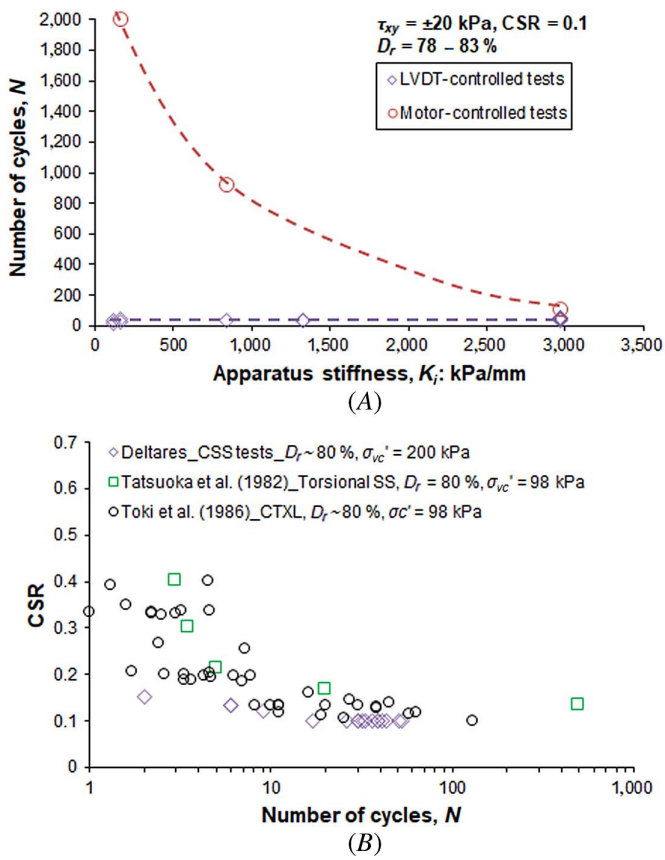

appear to merge to a satisfactory degree, providing a high level of confidence in the validity of the LVDT-controlled tests performed in this study. It should be noted that in **figure 8B** the cyclic stress ratio of the isotropically consolidated triaxial tests, CSR_{TX}, was related to the cyclic stress ratio of the simple shear tests, CSRss, via the Idriss and Boulanger (2008) relationship:

$$CSR_{SS} = \left(\frac{1 + 2 \cdot K_0}{3}\right) \cdot CSR_{TX} \tag{5}$$

The K_0 value in equation (5) is taken to be equal to $1 - \sin\phi'$. This value is obtained via Jaky's solution for a K_0 and an internal friction angle mobilized along the FL of $\phi'_{FL} = 29.8°$ (see **fig. 6**).

The remarkable stiffness-dependent cyclic response of the samples observed in **figure 7B** is explored in detail in **figure 9**. **Figure 9A** shows the change in vertical stress during cyclic loading for the case of samples tested under three different spring setting combinations (no springs, setting A, and setting B). The change in vertical stress is plotted versus time from the start of shearing up to failure of the samples, defined as the number of cycles required to reach a single amplitude shear strain of $\gamma_{SA} = 5\%$. Alternatively, the vertical stress development in **figure 9A** can be interpreted as a function of loading cycles, considering that for the testing frequency of 0.1 Hz a time interval of 10 s corresponds to one loading cycle. For the tests presented, the internal axial strain, $\Delta\varepsilon_{axial,i}$, is maintained constant via motor height control as shown in **figure 9B**. In contrast, the external axial strain,

FIG. 9 Motor-controlled direct simple shear tests on Toyoura sand samples performed on apparatus DSS A for different spring settings at $D_r \sim 80$ % and $\tau_{xy} = \pm 20$ kPa. Variation of (*A*) effective vertical stress, σ'_v; (*B*) internal axial strain, $\Delta\varepsilon_{axial,\,i}$; and (*C*) external axial strain, $\Delta\varepsilon_{axial,\,e}$, during cyclic loading.

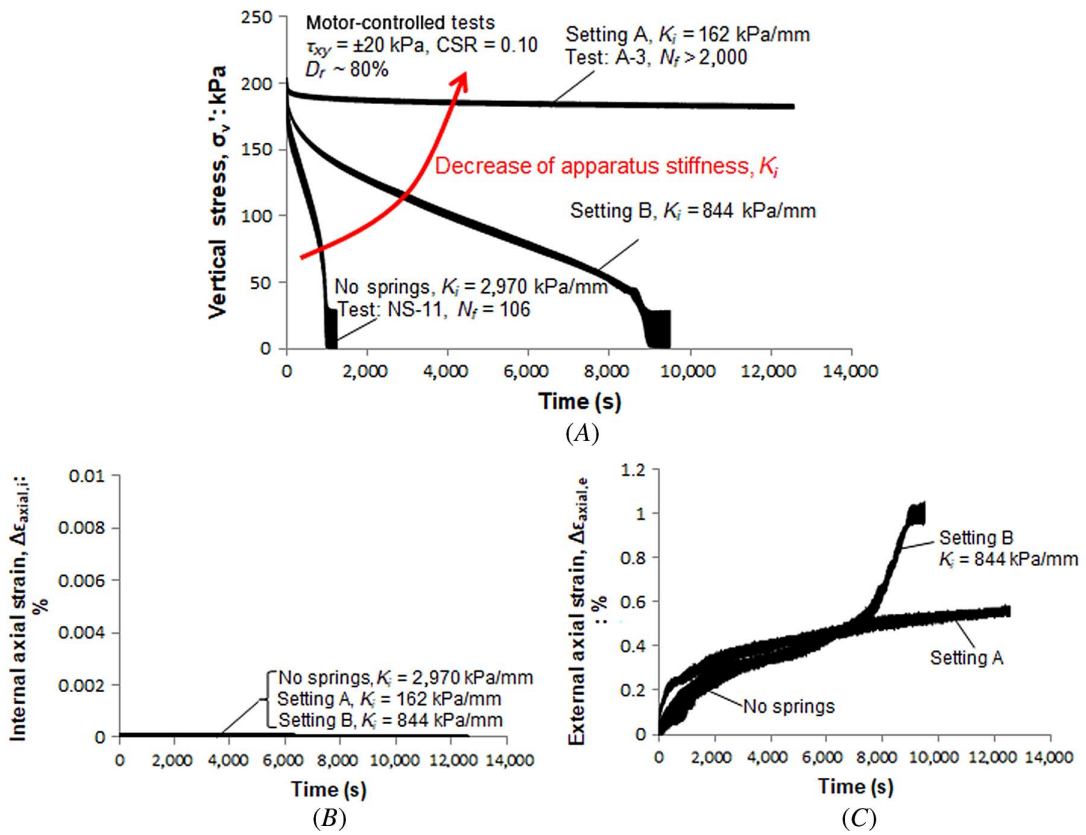

$\Delta\varepsilon_{axial,e}$, measured with the LVDT, accumulates during cyclic loading with the maximum recorded $\Delta\varepsilon_{axial,e}$ value reaching the level of 1 %.

It becomes apparent in **figure 9A** that the rate of change of the vertical stress imposed to the samples during cyclic loading for the same cyclic shear stress amplitude ($\tau_{xy} = \pm 20$ kPa) decreases with decreasing the apparatus stiffness, K_i. A lower rate of vertical stress change, or in other words a softer apparatus response, results in samples failing at a higher number of loading cycles. This observation highlights that the key to understanding the response of the samples to CDSS relies primarily on understanding the mechanism behind the development of vertical stress during shearing of the samples. It is evident that the amplitude of the vertical stress controls the resistance to cyclic loading, whereas this amplitude appears to be related to the stiffness of the apparatus components as shown in **figure 1**. In hindsight, the results are quite understandable. For the setting with springs, the stiffness of the apparatus is (much) lower than the stiffness of the sample. Consequently, volume change that is due to the cyclic loading will not lead to an unloading of the sand sample as could be expected with a completely stiff apparatus, but to some axial deformation of the apparatus and only a limited unloading. For example, if we assume a stiffness of the sand sample, K_s, of 3,200 kPa/mm and a stiffness of the apparatus of 800 kPa/mm, then it can be calculated with equation (3) that the unloading, i.e., in the first loading cycle, will roughly be 1/5 of the unloading in a completely stiff apparatus.

The validity of the conclusion that the stiffness is important is examined in **figure 10**, which presents the vertical stress (**fig. 10A**), internal axial strain (**fig. 10B**), and external axial strain (**fig. 10C**) development with time for the case of LVDT-controlled tests performed on samples having different spring settings (no springs, setting A, setting B, and setting C).

For the motor height control conditions, the internal apparatus stiffness, K_i, is of relevance because it expresses the reaction of the apparatus components within the motor height control area. For the LVDT-controlled

FIG. 10 LVDT-controlled direct simple shear tests on Toyoura sand samples performed on apparatus DSS A for different spring settings at $D_r \sim 80$ % and $\tau_{xy} = \pm 20$ kPa. Variation of (*A*) effective vertical stress, σ'_v; (*B*) internal axial strain, $\Delta\varepsilon_{axial,i}$; (*C*) external axial strain, $\Delta\varepsilon_{axial,e}$, during cyclic loading.

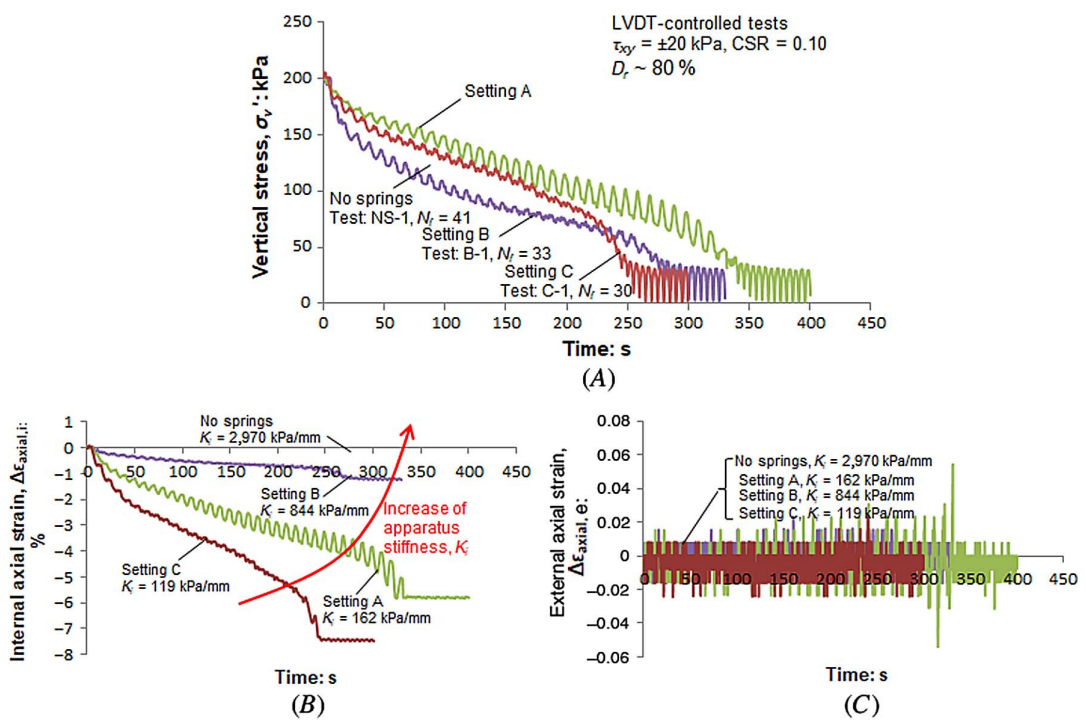

tests, however, the apparatus stiffness of interest is the one activated within the measurement area of the LVDT, denoted as K_3 in figure 1 and Table 2. Any changes in the rate of vertical stress reduction in figure 10*A* should reflect changes in the value of K_3 stiffness per spring setting combination. Nevertheless, as indicated in Table 2, K_3 has an almost constant value, irrespective of the spring conditions. This justifies the similar vertical stress response of the tested samples in figure 10*A*.

According to the external axial strain measurements in figure 10*C*, the height within the LVDT measurement area is controlled with an accuracy of ± 0.03 % during cyclic loading, whereas the apparatus stiffness, K_i, appears to control the internal axial strain response of the system (fig. 10*B*). Similar conclusions are drawn for all the LVDT-controlled tests performed in this study.

PREDICTION OF CYCLIC RESPONSE OF DENSE TOYOURA SAND SAMPLES TESTED UNDER LVDT AND MOTOR CONTROL HEIGHT CONDITIONS FOR DIFFERENT APPARATUS STIFFNESSES

In figure 11, the vertical stress development with time is plotted for the critical first loading cycle of five LVDT height control samples tested under identical conditions ($D_r \sim 80$ %, $\tau_{xy} = \pm 20$ kPa). A good repeatability of the measurements is evident with the vertical stress reduction at the end of the first loading cycle, $\Delta\sigma_{v(N=1)}^{\prime(LVDT)}$, receiving in average a value of 22 kPa. The vertical stress reduction mobilizes for each loading cycle a displacement of the LVDT, Δx_e, which is considered to be the sum of three different displacements, namely, the elastic displacement of the load piston, $\Delta x_{K_3}^{el}$, the elastic displacement of the sample, Δx_s^{el}, and the plastic displacement of the sample, Δx_s^{pl}. Overall, Δx_e, can be expressed as follows:

$$\Delta x_e = \Delta x_{K_3}^{el} + \Delta x_s^{el} + \Delta x_s^{pl} \tag{6}$$

In an LVDT-controlled test $\Delta x_e^{(LVDT)} = 0$. This means that

$$|\Delta x_s^{pl}| = \Delta x_{K_3}^{el} + \Delta x_s^{el} \tag{7}$$

Alternatively, equation (7) can be rewritten as

$$|\Delta x_s^{pl}| = \Delta\sigma_v^{\prime(LVDT)} \cdot \left(\frac{1}{K_3} + \frac{1}{K_s}\right) \tag{8}$$

Under motor-controlled conditions, the magnitude of the vertical stress reduction in the system, $\Delta\sigma_v^{\prime(Motor)}$, depends on the stiffness of the apparatus components K_1, K_2, and K_3 expressed for each spring setting

FIG. 11

Variation in vertical effective stress, σ_v', during the first loading cycle; LVDT-controlled direct simple shear tests on Toyoura sand samples performed on apparatus DSS A at $D_r \sim 80$ % and $\tau_{xy} = \pm$ 20 kPa.

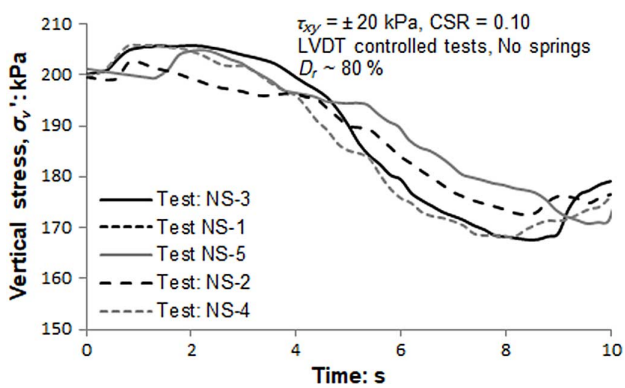

combination by the K_i stiffness (see **Table 2**). Under the assumption that the plastic deformation of the sample at the first loading cycle as given by equation (8) remains the same regardless of the imposed height-controlled conditions, the vertical stress reduction, $\Delta\sigma'^{(Motor)}_{v(N=1)}$, is predicted via the following equation:

$$\Delta\sigma'^{(Motor)}_{v(N=1)} = |\Delta x_s^{pl}| \cdot \frac{1}{\left(\frac{1}{K_s} + \frac{1}{K_i}\right)} \tag{9}$$

By substituting equation (8) into equation (9), it is obtained that

$$\Delta\sigma'^{(Motor)}_{v(N=1)} = \Delta\sigma'^{(LVDT)}_{v(N=1)} \cdot \left(\frac{1 + \frac{K_s}{K_3}}{1 + \frac{K_s}{K_i}}\right) \tag{10}$$

Using equation (10), the predicted vertical stress distribution during the first loading cycle is plotted against the experimental data in dashed line in **figure 12*A***, **12*C***, and **12*E*** for the case of a test with no springs, spring setting A, and spring setting B, respectively. The same methodology is applied to the test data up to 20 loading cycles, and the results are illustrated in **figure 12*B***, **12*D***, and **12*F***. It should be noted that the sample stiffness, K_s, as measured per test basis in **figure 12**, is applied in equation (10).

Overall, in **figure 12**, the measured and expected vertical stress distribution trend merge to a satisfactory degree. This conclusion signifies the importance of the apparatus stiffness, K_i, on the cyclic loading response for tests performed under motor-controlled conditions. This stiffness essentially acts as the driving force determining the amplitude of vertical stress reduction applied to the samples; the higher the value, the greater the vertical stress reduction is, leading to a lower sample resistance to cyclic loading.

It should be emphasized that equation (10) is considered to be more reliable when applied to the test data of the first loading cycle. At higher loading cycles, the sample's stiffness decreases and the actual stress-strain conditions imposed on the sample under motor control testing might influence the computation of the sample displacement given in equation (9).

In the case of LVDT-controlled tests, the vertical stress reduction, $\Delta\sigma'^{LVDT}_v$, during cyclic loading induces vertical displacements in the part of the apparatus above the LVDT (K_1 and K_2 components), which can be directly calculated by considering the activated effective stiffness $K_{eff}^{(K_1+K_2)}$ (**Table 2**). Under LVDT height control, any external displacement, Δx_e, is prohibited. For this to take place, the activated internal displacement, Δx_i, should be of such magnitude to counteract the deformation tendency of the K_1 and K_2 components triggered by the $\Delta\sigma'^{LVDT}_v$ reduction and expressed as

$$\Delta x_{i(N=1..i)} = \frac{\Delta\sigma'^{LVDT}_{v(N=1..i)}}{K_{eff}^{(K1+K2)}} \tag{11}$$

where i is the number of cycles to failure of the samples.

Based on equation (11), the predicted internal vertical displacement for samples with different spring settings (no springs, setting A, setting B, and setting C) is plotted against the experimental, Δx_i, measurements in **figure 13**. It appears that equation (11) sufficiently captures the development of Δx_i as cyclic loading progresses. It should be noted that for the case with no springs in **figure 13*A***, the measured and predicted Δx_i values deviate. The magnitude of this deviation, however, is minimal and in the order of 10^{-2} mm.

The magnitude of the Δx_i values in **figure 13** reflects the variations in the stiffness of the apparatus with higher values recorded per loading cycle as the effective stiffness $K_{eff}^{(K_1+K_2)}$ decreases.

Figure 14 presents the relationship between the measured internal vertical displacement and the vertical stress reduction $\Delta\sigma'^{LVDT}_v$ during cyclic loading for different spring combinations. As expected, this relationship is

FIG. 12 Motor-controlled direct simple shear tests on Toyoura sand samples performed on apparatus DSS A for different spring settings at $D_r \sim 80$ % and $\tau_{xy} = \pm 20$ kPa. Measured and predicted variation of effective vertical stress, σ'_v, during (*A*), (*C*), (*E*) the first loading cycle and (*B*), (*D*), (*F*) the first 20 loading cycles.

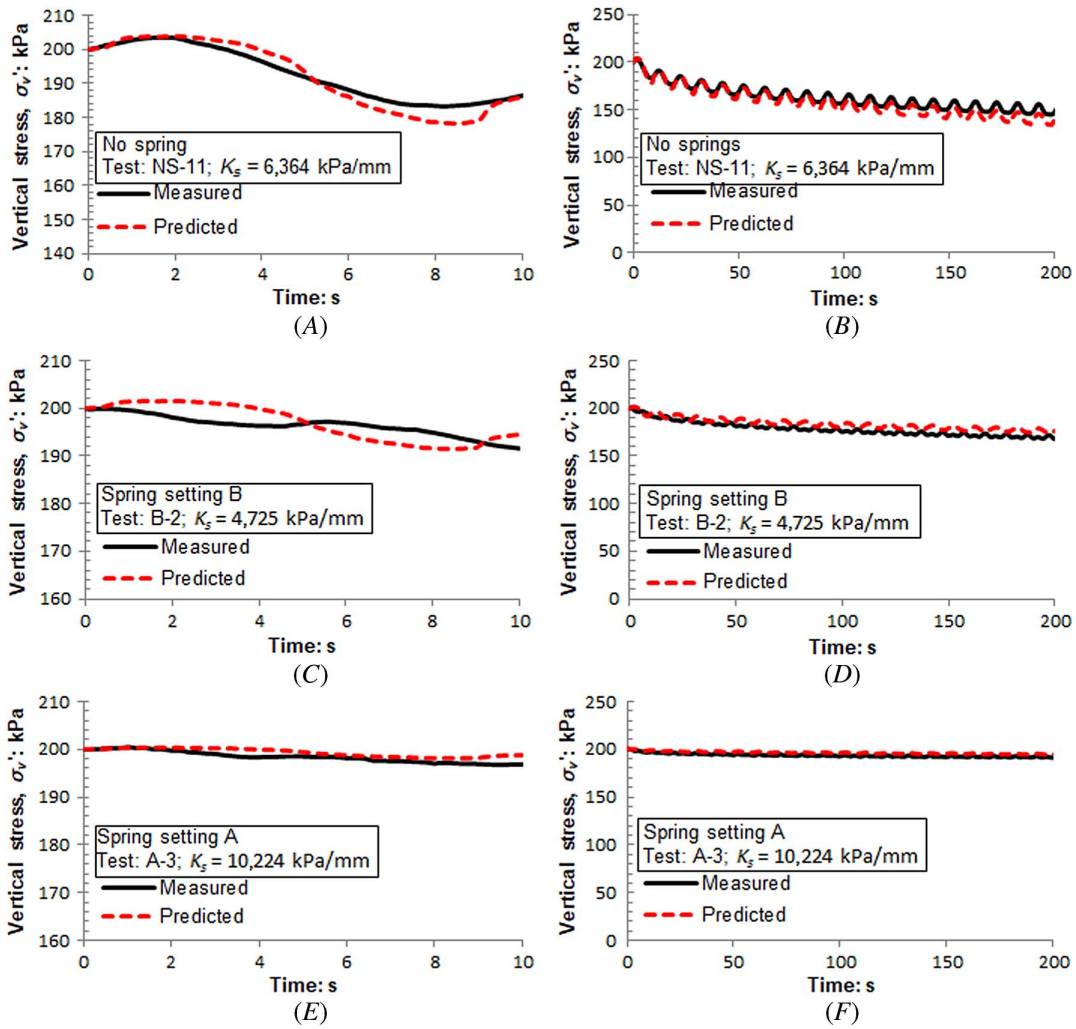

of a linear form and yields effective stiffness values $K_{eff,LVDT}^{(K_1+K_2)}$ that are remarkably similar to the $K_{eff}^{(K_1+K_2)}$ values as these are assessed from the compliance curves in figure 4.

COMPARISON OF CYCLIC STRENGTH RESISTANCE BETWEEN DENSE TOYOURA SAND SAMPLES ENCLOSED WITH REINFORCED MEMBRANE AND RING STACKS

According to ASTM D6528 in DSS tests, the sample can be laterally confined using either a wire-reinforced membrane (Bjerrum and Landva 1966) or stack of thin rings (Kjellmann 1951). The cyclic strength resistance curves as obtained from LVDT-controlled tests performed on dense Toyoura sand samples using both confinement methods are compared in figure 15. The inset photos in this figure show samples set up in both types of confinement methods. It can be observed that the applied method of confinement has a considerable impact on the cyclic undrained strength, which increases by about 50 % when a wire-reinforced membrane is used instead of a stack of thin rings. It should be emphasized that, to the authors' knowledge, no direct comparisons have been

FIG. 13 LVDT-controlled direct simple shear tests on Toyoura sand samples performed on apparatus DSS A at D_r ~80 % and $\tau_{xy} = \pm$ 20 kPa. Measured and predicted variation of internal vertical displacement, Δx_i, for (*A*) no springs; (*B*) spring setting B; (*C*) spring setting A; and (*D*) spring setting C.

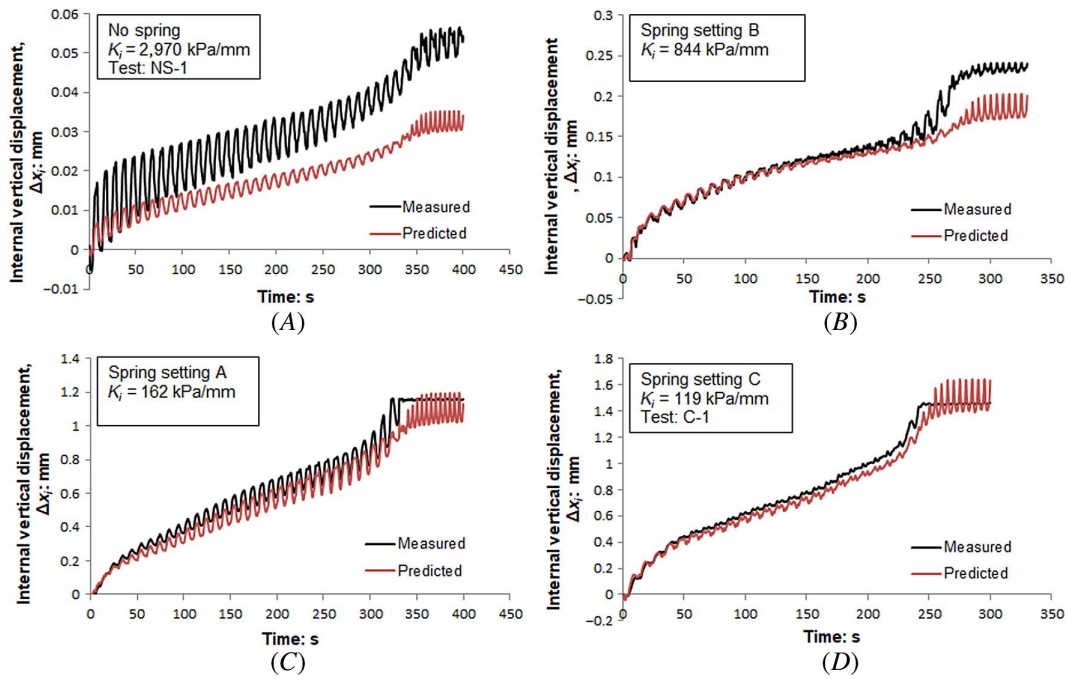

made in the literature to date in regard to the cyclic simple shear behavior of the two confinement methods. It may be possible that this result is caused by a different stiffness of the system but now in the horizontal direction. This will be investigated in the next section.

VOLUME AND AXIAL STRAIN GENERATION OF DENSE TOYOURA SAND SAMPLES DURING CONSOLIDATION AND CYCLIC LOADING

Volume change measurements have seldom been measured during the consolidation and shearing phase of a direct simple shear test. To evaluate whether the condition of constant volume is valid during constant height simple shear tests, volume measurements were recorded during consolidation and shearing of two samples tested with a wire - reinforced membrane (tests NS-14, NS-15) and one sample tested with ring stacks (test NS-4). The volume change and axial strain built up during consolidation of these samples is presented in **figure 16*A*** and **16*B***, respectively, whereas **figure 16*C*** shows the development of volume change with the number of cycles during shearing of the samples up to reaching failure. Note that in **figure 16** a positive volume change corresponds to a volume reduction of the sample.

It is noteworthy that the samples confined in the wire-reinforced membrane have higher strains during consolidation compared with the rings. Similar findings have been reported by Baxter et al. (2010) who concluded that the rings may provide increased lateral stiffness relative to the wire membranes. It should be pointed out, however, that in this study all tests were consolidated to a vertical stress level of 200 kPa. This consolidation stress level is only 20 % of the vertical stress capacity for the type of reinforced membrane used, indicating that the wire-reinforced membrane should have provided adequate lateral stiffness. Another possible cause for the observed differences in axial strains might be an increase in resistance to vertical load of the ring stacks and the unreinforced membrane surrounding the sample compared with the wire-reinforced membrane.

FIG. 14 Relationship between internal vertical displacement, Δx_i, and effective vertical stress reduction, $\Delta\sigma'_v$, during LVDT controlled cyclic loading of dense Toyoura sand samples performed on apparatus DSS A at $D_r \sim 80$ % and $\tau_{xy} = \pm$ 20 kPa. Test results for (*A*) no springs, test NS-1; (*B*) spring setting B, test B-1; (*C*) spring setting A, test A-2; (*D*) spring setting C, test C-1.

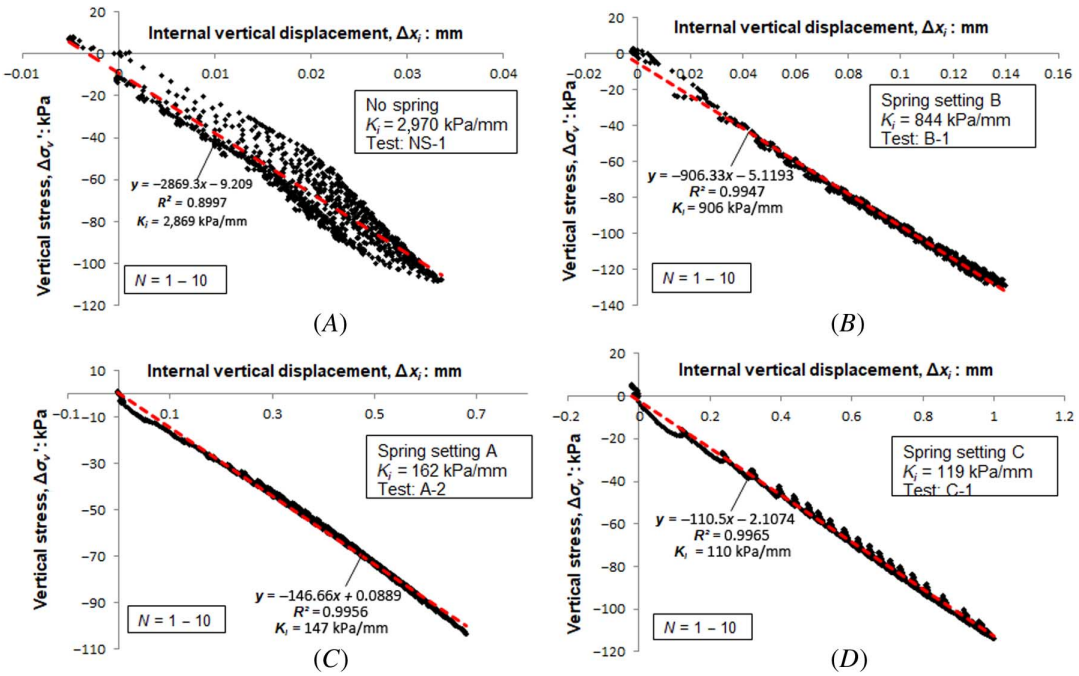

FIG. 15

Comparison between cyclic strength resistance curves of samples laterally confined with wire-reinforced membrane and ring stacks; LVDT-controlled direct simple shear tests on dense ($D_r \sim 80$ %) Toyoura sand samples performed on apparatus DSS A and DSS B.

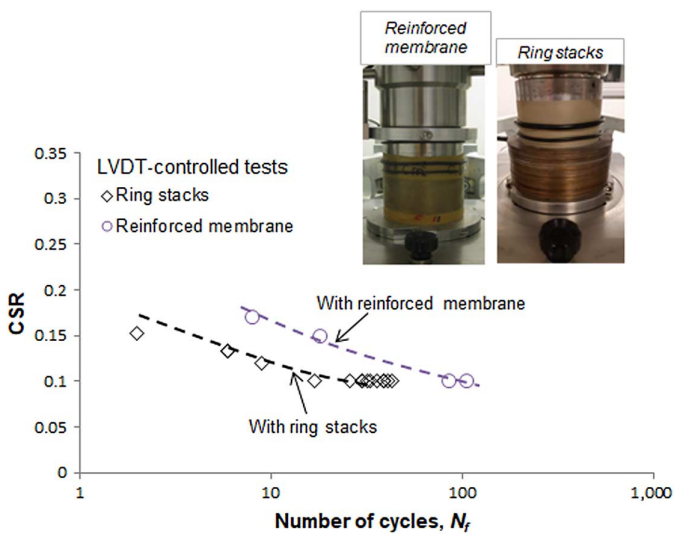

Because both wire-reinforced membrane and ring stacks prohibit lateral deformation of the soil sample, the measured volume changes during consolidation should in theory be, for the same vertical stress increments, identical to the axial strain measurements. The test data in figure 16*A* and 16*B* diverge from the expected

FIG. 16 Variation in (*A*) volume change, $\Delta\varepsilon_v$, and (*B*) external axial strain, $\Delta\varepsilon_{axial,\,e}$, with effective vertical stress, σ_v', during consolidation; (*C*) relation between volume change, $\Delta\varepsilon_v$, and number of cycles, *N*, during cyclic loading of LVDT-controlled dense Toyoura sand samples performed on apparatus DSS A.

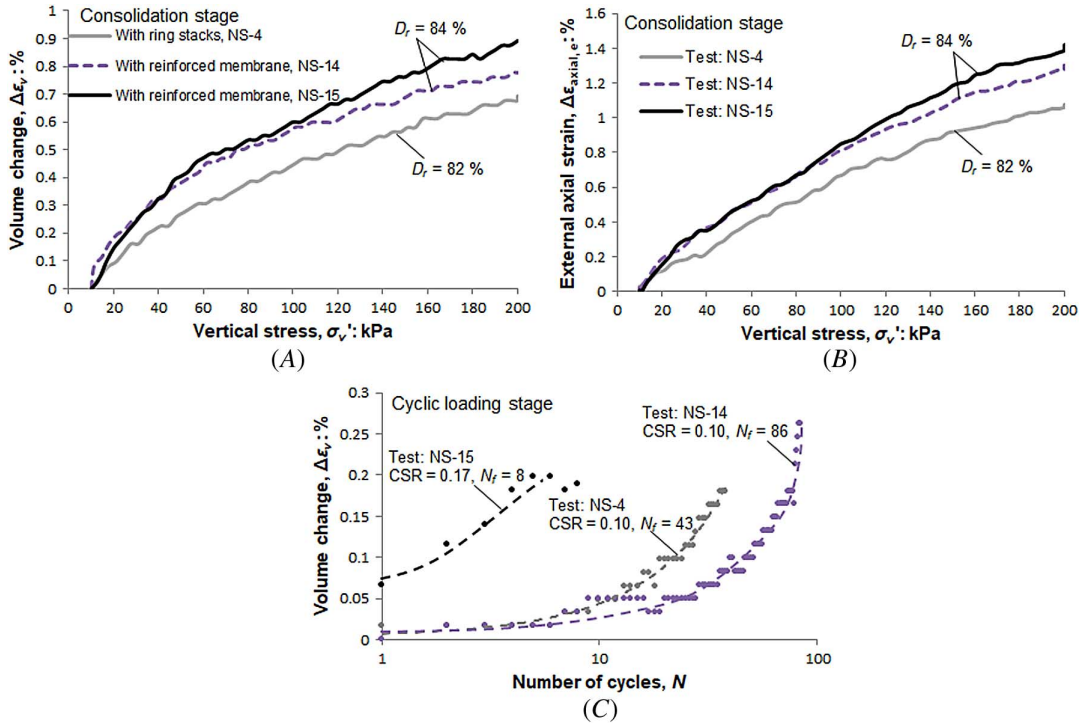

theoretical trend as the difference between the axial strain, $\Delta\varepsilon_{axial,e}$, and volume change of the samples, $\Delta\varepsilon_v$, is not negligible but increases almost linearly with vertical stress (fig. 17). In addition, the recorded volume change of the samples in figure 16C progressively increases with the number of loading cycles, reaching a value at failure in the range of 0.2–0.26 %. This indicates that true constant volume conditions are not achieved despite the fact that adequate LVDT conditions are applied and the height within the LVDT measurement area is maintained constant during cyclic loading (see fig. 10C). The behavior in figures 16C and 17 is attributed to the presence of the K_3 component stiffness.

On the ideal situation that during cyclic loading the volume change of the soil sample is zero, the plastic deformation of the sample, $\Delta\delta_s^{pl}$, should be compensated by its elastic deformation, $\Delta\delta_s^{el}$:

$$\Delta\delta_s^{pl} = -\Delta\delta_s^{el} \tag{12}$$

where

$$\Delta\delta_s^{el} = \frac{\Delta\sigma_{v,t}'}{K_s} \tag{13}$$

and $\Delta\sigma_{v,t}'$ is the vertical stress reduction during cyclic loading that would theoretically have been developed under the assumption that the elastic properties of the sample remain unchanged and the stiffness, K_3, of the load piston component can be neglected.

FIG. 17

Variation of the difference between axial strain and volume change increments, $\Delta\varepsilon_{axial,e} - \Delta\varepsilon_v$, with vertical effective stress, σ_v'; tests performed on apparatus DSS A.

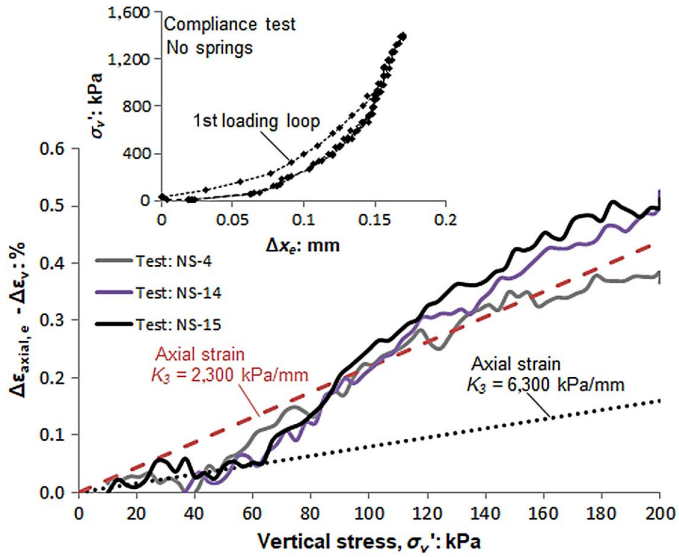

FIG. 18 Measured and predicted volume change, $\Delta\varepsilon_v$, against number of cycles, N, for (*A*) test NS-14 at CSR = 0.10; (*B*) test NS-4 at CSR = 0.10; (*C*) test NS-15 at CSR = 0.17; (*D*) variation of the difference between measured and predicted volume change, $\Delta\varepsilon_v$, as a function of number of cycles, N, for tests NS-4, NS-14, and NS-15 performed on apparatus DSS A.

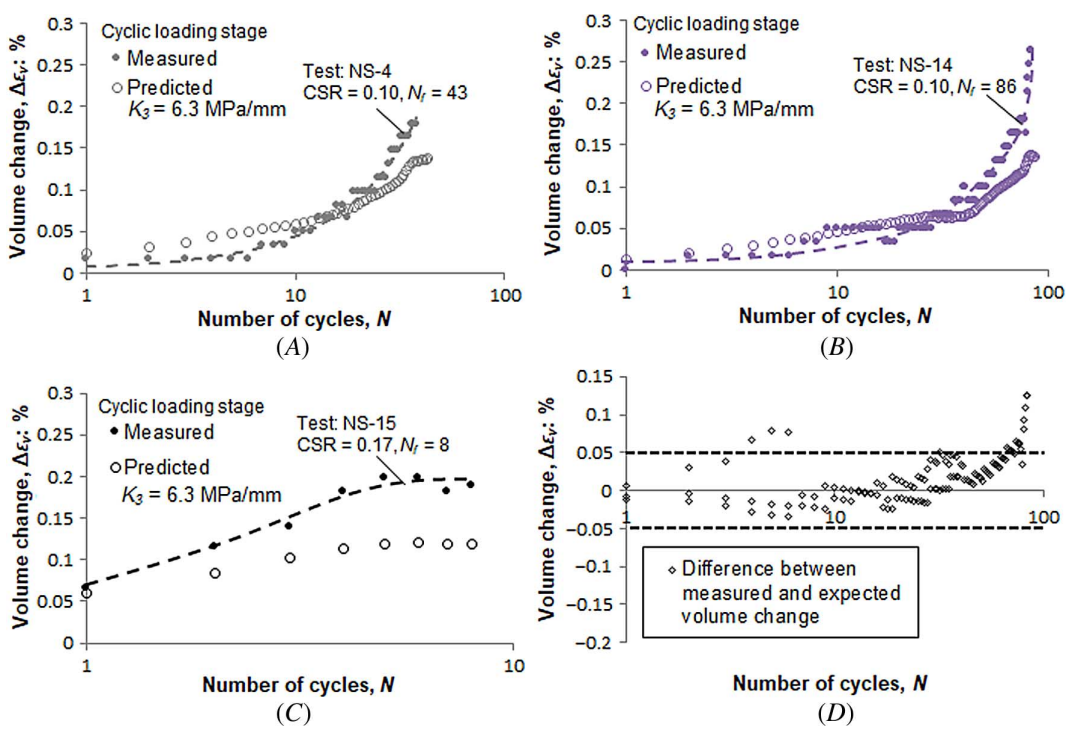

By substituting equation (13) into equation (8), it is obtained that

$$\Delta\sigma'_{v,t} = \Delta\sigma'_{v,m} \cdot \left(1 + \frac{K_s}{K_3}\right) \tag{14}$$

where $\Delta\sigma'_{v,m}$ represents the measured vertical stress reduction. Equation (14) shows that in reality the measured $\Delta\sigma'_{v,m}$ equals the calculated stress reduction in the case of no volume loss, $\Delta\sigma'_{v,t}$, only when the stiffness ratio $\frac{K_s}{K_3}$ is significantly low. Otherwise, $\Delta\sigma'_{v,t} > \Delta\sigma'_{v,m}$, and the volume change of the sample is indirectly proportional to the K_3 component stiffness as follows:

$$\Delta\delta_s = \frac{\Delta\sigma'_{v,m}}{K_3} \tag{15}$$

The volume change test data in this study together with the predicted data using equation (15) are illustrated for comparison in **figure 18*A–C***. The use of this equation appears to provide reliable volume change predictions that are in satisfactory agreement with the measured volume change pattern. As can be seen in **figure 18*D***, the difference between the measured and predicted volume change data fluctuates within the relatively small range of ±0.05 %.

The volume change of the samples during consolidation as predicted by equation (15) is also plotted with a black dotted line in **figure 17**. If the stiffness of the apparatus, expressed via the K_3 factor, is accountable for the volume change of the samples, it is to be expected that the $\Delta\varepsilon_{axial,e} - \Delta\varepsilon_v$ difference in **figure 17** should coincide with the volume change values given by equation (14) for a K_3^{aver} value of 6,300 kPa/mm, as this is determined from compliance tests (**fig. 4*B*** and **4*D***). This, however, is not evident in **figure 17** according to which the experimental data are best fitted with equation (15) for a lower stiffness value of $K_3 = 2{,}300\text{kPa/mm}$. It should be pointed out that the first loading part of the compliance curves (increase of vertical stress from 10 to 1,400 kPa) is omitted from the test data presented in **figure 4**. For this loading part, which reflects the apparatus stiffness during the consolidation stage of the samples, the response of the system is less stiff as can be seen in the inset diagram in **figure 17**; a K_3 value of 2,300 kPa/mm is calculated at the stress level of $\sigma'_v = 200$ kPa. A possible cause for this behavior could be a hidden flexibility in the system at the preparation stage, which is abolished at the presence of a first-time contact force. The first loading part is neglected from the calculation of the apparatus stiffnesses given in **Table 2** as it is considered not representative of the actual stiffness conditions that would occur in the testing phases of the samples after consolidation; for these phases, a $K_3 = 6{,}300\text{kPa/mm}$ is used. Nevertheless, when referring to the stiffness of the apparatus during the consolidation phase, it might be better to assume that the stiffness, K_3, has a lower value ($K_3 = 2{,}300\text{kPa/mm}$).

Discussion

According to Dyvik and Suzuki (2019), an active height control DSS device is a device in which the height of the sample alone is controlled and kept constant with a relatively high accuracy. To achieve this, direct displacement measurements are required over the sample. Such active height control devices are ideal. It is expected, however, that for the majority of the active and passive height control devices in use today the ability to maintain a constant sample height will depend on the stiffness of the device components that are included within the height control measurement area. For these devices, it is important to investigate what effect stiffness variations have on the results of DSS tests. This study provides experimental data and an interpretation methodology for quantifying this effect for the case of CDSS tests on dense sand samples.

The ASTM committee acknowledges the importance of system compliance; hence, ASTM D6528 states that for an undrained monotonic constant volume test, the DSS device shall not allow a sample change in height of more than 0.05 %. The basis of this allowable limit is uncertain. The test results herein demonstrate

the significance of equipment compliance in CDSS testing and suggest that even a height change of 0.05 % can significantly affect the measured shear and vertical effective stress. For the purposes of this work, a wide range of apparatus stiffnesses is intentionally used, which in combination with applied load levels results in sample height deviations that exceed the criterion of 0.05 %. The tests presented in this article serve therefore only in obtaining a better understanding on the influence that apparatus stiffness has on the CDSS test results. It should be realized that the 0.05 % criterion for a sample height of 20 mm, as typically used in DSS testing, corresponds to a maximum allowable vertical displacement of 0.01 mm. The necessary apparatus stiffness for this displacement and a pressure drop of, for example, 200 kPa should be at least 20,000 kPa/mm. To the authors' knowledge, the DSS devices in use today are unable to satisfy such high stiffness requirements. In addition, Zekkos et al. (2018) and Zehtab et al. (2019) conclude that a sample height change, even if it is limited to the value prescribed by ASTM D6528, can still significantly affect the monotonic and CDSS response of sand samples.

Equations (14) and (15) show that for a given height change limit, the effect of system compliance on the results of constant volume DSS tests depends primarily on the stiffness of the tested sample; the higher the sample stiffness is, the higher will be the deviations in behavior compared with samples tested under truly constant height conditions. Consequently, the adoption of a unique sample height change limit can lead to misleading results especially in DSS testing of very stiff materials such as dense sands.

A similar conclusion can be found in the study of Dyvik and Suzuki (2019) who performed monotonic constant volume DSS tests on different types of materials for evaluating the effect of sample height change on the test results. They observed that the sample height effect is greater for the stiffer soil samples.

In conclusion, two factors should be thoroughly considered when interpreting CDSS test results: device stiffness within the height control area, K_{device}, and the stiffness of the tested sample, K_s. For more realistic estimates of liquefaction potential for the case of sand samples, a better approach will be the adoption by ASTM D6528 of a unique K_s/K_{device} ratio criterion rather than a sample height change limit. For performing a DSS test to the closest proximity to constant volume conditions, the K_s/K_{device} ratio should have a considerably low value, the magnitude of which can be defined on the basis of a known effect on DSS test results.

Conclusions

The stiffness of the DSS apparatus is of major importance as it proved to control the cyclic behavior of the dense Toyoura sand samples in this study. The resistance to liquefaction is shown to increase as the apparatus stiffness decreases. In ideal DSS testing, truly constant volume conditions can be achieved with active height control of the sample itself. In this case, the apparatus stiffness is not a factor to be considered. Contrastively, for the active and passive height control devices in use today, the quality of the test results depends on the stiffness of the equipment. For these devices, the stiffness-dependent response of the sand samples shown in this study is of paramount importance and should not be neglected in the interpretation of CDSS results. Failure to account for the influence of the apparatus stiffness may yield inconsistencies in the comparison of CDSS tests performed by different devices. The results from this study suggest that the stiffness of the apparatus elements within the height control measurement area need to be designed to minimize compliance. In this perspective, LVDT (active)-controlled tests are recommended in this article over motor (passive)-controlled tests.

For both types of height control techniques (active and passive), ASTM D6528 specifies that the height of the sample during shear should not deviate by more than 0.05 % of its preshear value. This height change limit fails, however, to account for the effect of sample stiffness on the DSS test results. Based on the findings from this study, this effect can be significant when testing involves very stiff samples such as is the case of dense sands. It seems thus meaningful to interpret the results of DSS tests on the basis of a stiffness of the tested sample to the stiffness of the apparatus ratio criterion rather than a sample height change limit.

The effect of equipment compliance on the DSS test results can be reduced within certain tolerated limits if the ratio of the sample's stiffness to the stiffness of the apparatus remains significantly low. For those passive

height control devices in use today that prove to be unable to fulfill the previous ratio requirement, truly constant volume conditions can alternatively be achieved when the test is controlled by measuring the water volume expelled during testing via a balance of high accuracy.

The confinement method affects the cyclic undrained strength of dense Toyoura sand, which is about 50 % higher when a wire-reinforced membrane is used instead of ring stacks. In addition, samples confined with a wire-reinforced membrane exhibited more vertical strain to the effective consolidation stress than samples confined with stacked rings. It remains, however, unclear what is the true cause for the observed differences between the two confinement methods; hence, more research is required for reaching a definitive conclusion.

ACKNOWLEDGMENTS

The authors wish to thank Lambert Smidt, project technician, for his valuable contribution to this work.

References

Andersen, K. H. 2009. "Bearing Capacity under Cyclic Loading—Offshore, along the Coast, and on Land. The 21st Bjerrum Lecture Presented in Oslo, 23 November 2007." *Canadian Geotechnical Journal* 46, no. 5 (May): 513–535. https://doi.org/10.1139/T09-003

ASTM International. 2017. *Standard Test Method for Consolidated Undrained Direct Simple Shear Testing of Fine Grain Soils*. ASTM D6528-17. West Conshohocken, PA: ASTM International, approved August 1, 2017. https://doi.org/10.1520/D6528-17

Baxter, C. D. P., A. S. Bradshaw, M. Ochoa-Lavergne, and R. Hankour. 2010. "DSS Test Results Using Wire-Reinforced Membranes and Stacked Rings." In *GeoFlorida 2010*, 600–607. Reston, VA: American Society of Civil Engineers.

Bjerrum, L. and A. Landva. 1966. "Direct Simple-Shear Tests on a Norwegian Quick Clay." *Géotechnique* 16, no. 1 (March): 1–20. https://doi.org/10.1680/geot.1966.16.1.1

Boulanger, R. W. and R. B. Seed. 1995. "Liquefaction of Sand under Bidirectional Monotonic and Cyclic Loading." *Journal of Geotechnical Engineering* 121, no. 12 (December): 870–878. https://doi.org/10.1061/(ASCE)0733-9410(1995)121:12(870)

Cappellaro, C., M. Cubrinovski, G. Chiaro, M. E. Stringer, J. D. Bray, and M. F. Riemer. 2017. "Undrained Cyclic Direct Simple Shear Testing of Christchurch Sandy Soils." In *20th NZGS Geotechnical Symposium*, edited by G. J. Alexander and C. Y. Chin, 1–8. Wellington, New Zealand: New Zealand Geotechnical Society.

Castro, G. 1975. "Liquefaction and Cyclic Mobility of Saturated Sands." *Journal of the Geotechnical Engineering Division* 101, no. 6: 551–569.

Castro, G. and S. J. Poulos. 1977. "Factors Affecting Liquefaction and Cyclic Mobility." *Journal of the Geotechnical Engineering Division* 103, no. 6: 501–506.

Chiaro, G., J. Koseki, and T. Sato. 2012. "Effects of Initial Static Shear on Liquefaction and Large Deformation Properties of Loose Saturated Toyoura Sand in Undrained Cyclic Torsional Shear Tests." *Soils and Foundations* 52, no. 3 (June): 498–510. https://doi.org/10.1016/j.sandf.2012.05.008

Dyvik, R., T. Berre, S. Lacasse, and B. Raadim. 1987. "Comparison of Truly Undrained and Constant Volume Direct Simple Shear Tests." *Géotechnique* 37, no. 1 (March): 3–10. https://doi.org/10.1680/geot.1987.37.1.3

Dyvik, R. and Y. Suzuki. 2019. "Effect of Volume Change in Undrained Direct Simple Shear Tests." *Geotechnical Testing Journal* 42, no. 4 (July): 1075–1082. https://doi.org/10.1520/GTJ20170287

Finn, W. D., D. J. Pickering, and P. L. Bransby. 1971. "Sand Liquefaction in Triaxial and Simple Shear Tests." *Journal of the Soil Mechanics and Foundations Division* 97, no. 4: 639–659.

Georgiannou, V. N. and A. Tsomokos. 2008. "Comparison of Two Fine Sands under Torsional Loading." *Canadian Geotechnical Journal* 45, no. 12 (December): 1659–1672. https://doi.org/10.1139/T08-083

Idriss, I. M. and R. W. Boulanger. 2008. *Soil Liquefaction during Earthquakes, Monograph MNO-12*. Oakland, CA: Earthquake Engineering Research Institute.

Ishihara, K. and F. Yamazaki. 1980. "Cyclic Simple Shear Tests on Saturated Sand in Multi-directional Loading." *Soils and Foundations* 20, no. 1 (March): 45–59. https://doi.org/10.3208/sandf1972.20.45

Kim, Y.-S. 2009. "Static Simple Shear Characteristics of Nak-Dong River Clean Sand." *KSCE Journal of Civil Engineering* 13, no. 6 (September): 389–401. https://doi.org/10.1007/s12205-009-0389-9

Kiyota, T., T. Sato, J. Koseki, and D. Abadimarand. 2008. "Behavior of Liquefied Sands under Extremely Large Strain Levels in Cyclic Torsional Shear Tests." *Soils and Foundations* 48, no. 5 (October): 727–739. https://doi.org/10.3208/sandf.48.727

Kjellmann, W. 1951. "Testing the Shear Strength of Clay in Sweden." *Géotechnique* 2, no. 3 (June): 225–235. https://doi.org/10.1680/geot.1951.2.3.225

Konstadinou, M. and V. N. Georgiannou. 2013. "Cyclic Behaviour of Loose Anisotropically Consolidated Ottawa Sand under Undrained Torsional Loading." *Géotechnique* 63, no. 13 (October): 1144–1158. https://doi.org/10.1680/geot.12.P.145

Li, Y., Y. Yang, H.-S. Yu, and G. Roberts. 2017. "Monotonic Direct Simple Shear Tests on Sand under Multidirectional Loading." *International Journal of Geomechanics* 17, no. 1 (January): 04016038. https://doi.org/10.1061/(ASCE)GM.1943-5622.0000673

Matsuda, H., H. Shinozaki, N. Okada, K. Takamiya, and K. Shinyama. 2004. "Effects of Multi-directional Cyclic Shear on the Post-Earthquake Settlement of Ground." In *13th World Conference on Earthquake Engineering*, 2890. Vancouver, Canada: 13 WCEE Secretariat.

McGuire, S. T. "Comparison of Direct Simple Shear Confinement Methods on Clay and Silt Specimens." Master's thesis, University of Rhode Island, 2011.

Mulilis, J. P., K. Arulanandan, J. K. Mitchell, C. K. Chan, and H. B. Seed. 1977. "Effects of Sample Preparation on Sand Liquefaction." *Journal of the Geotechnical Engineering Division* 103, no. 2: 91–108.

Peacock, W. H. and H. B. Seed. 1968. "Sand Liquefaction under Cyclic Loading Simple Shear Conditions." *Journal of the Soil Mechanics and Foundations Division* 94, no. 3: 689–708.

Quinteros, V. S., T. Lunne, R. Dyvik, L. Krogh, R. Bøgelund-Pedersen, and S. Bøtker-Rasmussen. 2017. "Influence of Pre-shearing on the Triaxial Drained Strength and Stiffness of a Marine North Sea Sand." In *Eighth International Conference, Offshore Site Investigation Geotechnics*, 338–345. London: Society for Underwater Technology. https://doi.org/10.3723/OSIG17.338

Roscoe, K. H. 1953. "An Apparatus for the Application of Simple Shear to Soil Samples." In *Third International Conference on Soil Mechanics and Foundation Engineering*, 186–191. Zurich, Switzerland: ICOSOMEF Organizing Committee.

Tatsuoka, F., M. Muramatsu, and T. Sakaki. 1982. "Cyclic Undrained Stress-Strain Behaviour of Dense Sands by Torsional Simple Shear Test." *Soils and Foundations* 22, no. 2 (June): 55–70. https://doi.org/10.3208/sandf1972.22.2_55

Toki, S., F. Tatsuoka, S. Miura, Y. Yoshimi, S. Yasuda, and Y. Makihara. 1986. "Cyclic Undrained Triaxial Strength of Sand by a Cooperative Testing Program." *Soils and Foundations* 26, no. 3 (September): 117–128. https://doi.org/10.3208/sandf1972.26.3_117

Vaid, Y. P. and J. C. Chern. 1985. "Cyclic and Monotonic Undrained Response of Saturated Sands." In *Advances in the Art of Testing Soils under Cyclic Conditions*, 120–147. Reston, VA: American Society of Civil Engineers.

Vaid, Y. P. and S. Sivathayalan. 1996. "Static and Cyclic Liquefaction Potential of Fraser Delta Sand in Simple Shear and Triaxial Tests." *Canadian Geotechnical Journal* 33, no. 2 (May): 281–289. https://doi.org/10.1139/t96-007

Wijewickreme, D., S. Sriskandakumar, and P. Byrne. 2005. "Cyclic Loading Response of Loose Air-Pluviated Fraser River Sand for Validation of Numerical Models Simulating Centrifuge Tests." *Canadian Geotechnical Journal* 42, no. 2 (April): 550–561. https://doi.org/10.1139/t04-119

Zehtab, K., S. Gokyer, S. K. Werden, W. A. Marr, and A. Apostolov. 2019. "On the Effects of Inadequate Height Control in Constant Volume Monotonic and Cyclic Direct Simple Shear Test." In *Geo-Congress 2019*, 363–373. Reston, VA: American Society of Civil Engineers.

Zekkos, D., A. Athanasopoulos-Zekkos, J. Hubler, X. Fei, K. Zehtab, and W. Marr. 2018. "Development of a Large-Size Cyclic Direct Simple Shear Device for Characterization of Ground Materials with Oversized Particles." *Geotechnical Testing Journal* 41, no. 2 (March): 263–279. https://doi.org/10.1520/GTJ20160271